



ALMA MATER STUDIORUM
UNIVERSITÀ DI BOLOGNA

ARCHIVIO ISTITUZIONALE
DELLA RICERCA

Alma Mater Studiorum Università di Bologna Archivio istituzionale della ricerca

A Multi-port Power Conversion System for the More Electric Aircraft

This is the final peer-reviewed author's accepted manuscript (postprint) of the following publication:

Published Version:

Gu C., Yan H., Yang J., Sala G., De Gaetano D., Wang X., et al. (2020). A Multi-port Power Conversion System for the More Electric Aircraft. IEEE TRANSACTIONS ON TRANSPORTATION ELECTRIFICATION, 6(4), 1707-1720 [10.1109/TTE.2020.3019446].

Availability:

This version is available at: <https://hdl.handle.net/11585/778812> since: 2024-02-27

Published:

DOI: <http://doi.org/10.1109/TTE.2020.3019446>

Terms of use:

Some rights reserved. The terms and conditions for the reuse of this version of the manuscript are specified in the publishing policy. For all terms of use and more information see the publisher's website.

This item was downloaded from IRIS Università di Bologna (<https://cris.unibo.it/>).
When citing, please refer to the published version.

(Article begins on next page)

A Multi-port Power Conversion System for the More Electric Aircraft

Chunyang Gu, Hao Yan, Jiajun Yang, Giacomo Sala, Daniele De Gaetano, Xuchen Wang, Alessandro Galassini, Michele Degano, Xin Zhang, Giampaolo Buticchi



**University of
Nottingham**

UK | CHINA | MALAYSIA

University of Nottingham Ningbo China, 199 Taikang East Road, Ningbo, 315100, Zhejiang, China.

First published 2020

This work is made available under the terms of the Creative Commons Attribution 4.0 International License:

<http://creativecommons.org/licenses/by/4.0>

The work is licenced to the University of Nottingham Ningbo China under the Global University Publication Licence:

<https://www.nottingham.edu.cn/en/library/documents/research-support/global-university-publications-licence-2.0.pdf>



**University of
Nottingham**

UK | CHINA | MALAYSIA

A Multi-port Power Conversion System for the More Electric Aircraft

Chunyang Gu, *Member, IEEE*, Hao Yan, *Member, IEEE*, Jiajun Yang, *Student Member, IEEE*, Giacomo Sala, Daniele De Gaetano, Xuchen Wang, *Student Member, IEEE*, Alessandro Galassini, *Member, IEEE*, Michele Degano, *Member, IEEE*, Xin Zhang, *Senior Member, IEEE*, and Giampaolo Buticchi, *Senior Member, IEEE*

Abstract- In more electric aircraft (MEA) weight reduction and energy efficiency constitute the key figures. Additionally, the safety and continuity of operation of its electrical power distribution system (EPDS) is of critical importance. These sets of desired features are in disagreement with each other, because higher redundancy, needed to guarantee the safety of operation, implies additional weight. In fact, EPDS is usually divided into isolated sections, which need to be sized for the worst-case scenario. Several concepts of EPDS have been investigated, aiming at enabling the power exchange among separate sections, which allows better optimization for power and weight of the whole system. In this paper, an approach based on the widespread use of multi-port power converters for both DC/DC and DC/AC stages is proposed. System integration of these two is proposed as a multi-port power conversion system (MPCS), which allows a ring power distribution while galvanic isolation is still maintained, even in fault conditions. Thus, redundancy of MEA is established by no significant weight increase. A machine design analysis shows how the segmented machine could offer superior performance to the traditional one with same weight. Simulation and experimental verifications show the system feasibility in both normal and fault operations.

Index Terms- More electric aircraft, multi-port active bridge (MAB), electrical power distribution system, segmented driven starter/generators, multi-port power conversion system, Multi three-phase electrical machines.

Manuscript received March 10, 2020; revised June 05, 2020 and July 29, 2020; accepted August 15, 2020. This work was supported in part by National Natural Science Foundation of China under Grant 51807099, in part by Zhejiang Natural Science Foundation under Grant LQ19E070002 and in part by Ningbo Science & Technology Beauru under Grant 2018A610146 and 2018B10082. (*Corresponding author: Hao Yan*)

Chunyang Gu, Jiajun Yang, Xuchen Wang and Giampaolo Buticchi are with the Key Laboratory of More Electric Aircraft Technology of Zhejiang Province, University of Nottingham Ningbo China, Ningbo 315100, China (e-mail: Chunyang.Gu@nottingham.edu.cn; jiajun_yang@outlook.com; Xuchen.Wang@nottingham.edu.cn; Giampaolo.Buticchi@nottingham.edu.cn).

Hao Yan is with the School of Civil Aviation, Northwestern Polytechnical University, Xi'an 710000, China (e-mail: yanhaohit@yahoo.com).

Giacomo Sala is with the Department of Electrical, Electronic and Information Engineering "Guglielmo Marconi", University of Bologna, Italy (e-mail: giacomo.sala5@unibo.it).

Daniele De Gaetano, Alessandro Galassini and Michele Degano are with the Power Electronics, Machines and Control (PEMC) Research Group, University of Nottingham, NG7 2RD, U.K. (e-mail: eexdd6@exmail.nottingham.ac.uk; alessandro.galassini@nottingham.ac.uk; michele.degano@nottingham.ac.uk).

Xin Zhang is with the School of Electrical and Electronic Engineering, Nanyang Technological University, Singapore 639798, Singapore (e-mail: jackzhang@ntu.edu.sg).

NOMENCLATURE

MEA	More Electric Aircraft
EPDS	Electrical Power Distribution System
MPCS	Multi-port Power Conversion System
TRU	Transformer Rectifier Unit
APU	Auxiliary Power Unit
HVDC	High Voltage Direct Current
LVDC	Low Voltage Direct Current
MAB	Multiple Active Bridge
IPM	Interior Permanent Magnet
EMF	Electromotive Force
FE	Finite Element
PWM	Pulse Width Modulation
QAB	Quadruple Active Bridge
n	Number of H-bridges in an MAB
m	Number of phases for the machine
$V_{dc1}, V_{dc2}, V_{dc3}, V_{dc4}, V_{dc5}, \dots, V_{dc,n}$	DC voltages of an MAB (or a QAB)
$i_1, i_2, i_3, i_4, i_5, \dots, i_n$	High frequency AC currents of an MAB (or a QAB)
$v_1, v_2, v_3, v_4, v_5, \dots, v_n$	High frequency AC voltages of an MAB (or a QAB)
L_1, L_2, L_3, L_4	QAB transformer leakage inductances
C_1, C_2, C_3, C_4	QAB DC capacitances
f_{sw}	QAB switching frequency
d_{21}, d_{31}, d_{41}	Phase shift angles for the H-bridges of QAB
i_d, i_q	d-axis and q-axis currents
$i_{a1}, i_{b1}, i_{c1}; i_{a2}, i_{b2}, i_{c2}$	2×3-phase machine AC currents
$I_{dc1}, I_{dc2}, I_{dc3}, I_{dc4}$	DC port currents of a QAB
$P_{dc1}, P_{dc2}, P_{dc3}, P_{dc4}$	DC port powers of a QAB

I. INTRODUCTION

THE more electric aircraft (MEA) framework draws a lot of attention among the power electronic experts as it simultaneously belongs to the areas of smart power distribution, micro grids and transportation electrification. In the field of power distribution and micro grids, the increasing energy demand challenged the aircraft power distribution systems with strict requirements of safety and reliability [1]. The MEA concept envisages the substitution of the oil distribution with electro-mechanical actuators or even fully electrical actuators, further increasing the electric power requirements. In the field of transportation electrification, the development of power

generation, distribution, storage and advanced information communication have laid great foundation for the next generation of more electric aircrafts [2].

In the MEA, electrical generators usually employ 3-phase AC drives, albeit most of the loads are DC loads, or AC loads with different power/frequency requirements. Therefore, the so called Transformer-Rectifier Units (TRUs) are utilized in the MEA for feeding different loads [3]. The TRUs confer galvanic isolation and convert AC to DC by using rectifiers. Besides, AC, DC or hybrid buses are implemented in the MEA for power distribution.

To improve the weight/volume consumption and efficiency as well as increase the safety and availability of the electrical power distribution system (EPDS), this paper proposes multi-port power conversion systems (MPCSs) [4-7]. With this concept of multi-port power converters, both for the DC/DC stages (i.e. multiple active bridge converter) and for the DC/AC stages (segmented inverters), a ring distribution of the electrical power system featuring galvanic isolation properties among its redundant compartments is established.

In this paper, a system concept of MPCS based EPDS is proposed, by integrating multiple DC/DC converters together with segmented multiphase machine drives. The goal is to have an interconnected EPDS where the power can be exchanged across the whole system, and at the same time guaranteeing the resiliency thanks to the galvanic isolation of the DC/DC converters and of the machines. For the first time, the electrical machines and the converters become part of a complex power distribution structure, that shows resiliency and fault tolerance with little additional power/weight installed.

The concept is validated by both simulations and experiments. Section II describes the possible electrical distribution system paradigms and introduces the concept of multi-port power conversion systems, covering design and implementation aspects of multiport DC/DC and AC/DC converters. Section III illustrates the segmented multi-3-phase machine design guidance, as the key energy conversion component for multiport AC/DC converters. Section IV validates the proposed MPCS based EPDS by simulations during normal and faulty operation. Section V shows the experimental results obtained on a prototype system. Section VI draws the conclusions of the work, highlighting its most important achievements and contributions to the state of the art of the MEA.

II. MULTI-PORT POWER CONVERSION SYSTEM AS AN ELECTRICAL POWER DISTRIBUTION SYSTEM

Different types of load are considered in the MEA: fuel and oil pumps and micro turbines are AC loads, whereas actuators, battery storage systems and avionics are DC loads [8]. The mixture of both AC and DC loads requires a complicated structure of EPDSs where the main generators and auxiliary power units (APUs) supply the main DC bus. Different architectures of hybrid EPDSs have been analyzed in [9], concluding that a hybrid distribution with DC implementation and AC/DC rectifiers for the generators is the architecture with the smallest weight.

Fig. 1 compares two schematics of a distribution system. In Fig. 1(a), the generators are feeding a three-phase AC bus with variable frequency. The control of the excitation winding of the generators regulates a constant voltage amplitude. Two TRUs are used to provide the DC buses with a high voltage direct current (HVDC) at 270V, and a switching matrix allows for the connection of the APUs to the AC bus bars. In the case of a fault in one engine, the bus bars can also be connected together to keep the EPDS operational. Conversely, in Fig. 1(b) the generators are directly connected to AC/DC converters that provide the required power to the respective DC bus bars. AC loads are connected to the DC distribution via suitable DC/AC inverters. The low voltage direct current (LVDC) loads are connected to the main DC bus via isolated DC/DC converters.

Fig. 2 depicts an example of a DC-based EPDS with multi-port power converters. The DC/DC and DC/AC multi-port power converters are highlighted in yellow. Compared with Fig. 1(b), a multiport DC/DC converter (i.e. multiple active bridge converter, MAB) is replacing the two isolated DC/DC converters, and segmented starter/generators with segmented inverter configurations are placed instead of traditional generators with single inverters.

To implement the multi-port power conversion systems for the MEA, the configurations of both DC/DC multiple active bridge converters and the DC/AC segmented machines and inverters for starter/generators are described, followed by fault tolerant and communication considerations.

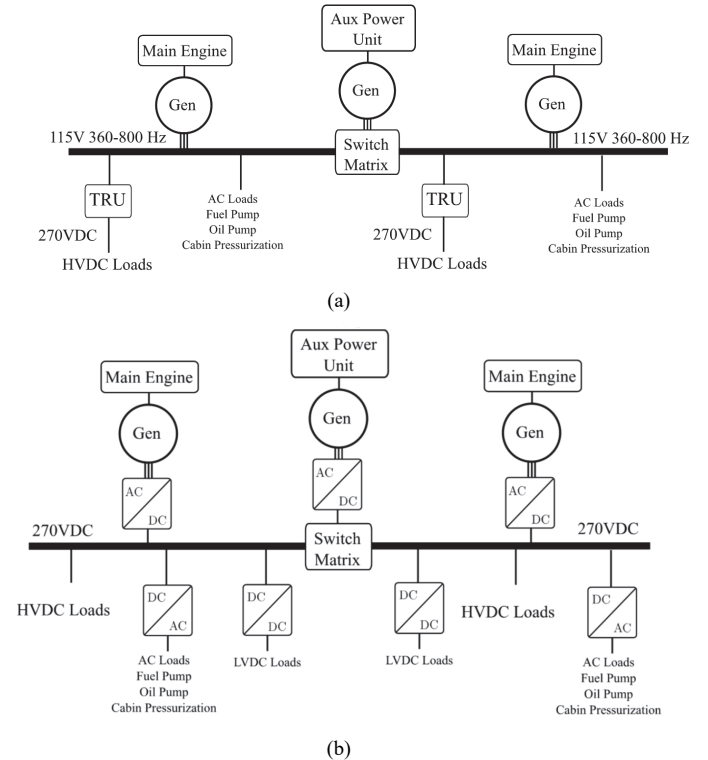


Fig. 1. Example of an hybrid electrical power distribution systems with AC (a) and DC (b) distribution.

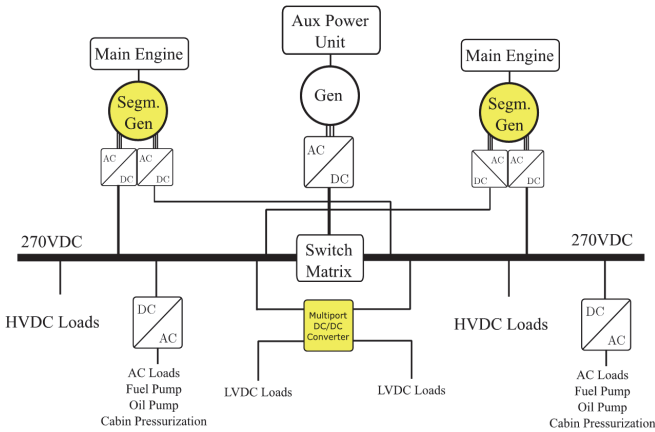


Fig. 2. Example of the proposed MPCS based EPDS.

A. DC/DC multiple active bridge converters

Fig. 3 illustrates the configuration of MAB converters [10–13], in which a group of high frequency inverters, high frequency rectifiers and a multi-winding transformer are involved. The number of windings of the multi-winding transformer is determined by the requirements of sources and loads. The MAB provides a multiport power-flow path for all the connected units. All windings of the transformer are linked by the same flux, therefore the power can be transferred naturally by the energy delivery within different windings through the common transformer flux. The major advantages of MAB are as follows:

- The efficiency and power density of MAB is higher than traditional TRUs according to its high frequency transformers [14].
- The voltage and power balancing are realized by flux linkage, so that the load of different windings of the transformer can be totally different from each other, giving flexibility and redundancy properties to the design [12].
- The power density of MAB is higher than separate DC/DC converters: multi-winding structure could decrease the size and weight of insulation by sharing the transformer flux linkage [15].
- The efficiency of MAB is higher than the separated configuration, because the sharing of the magnetizing current helps reducing the related copper loss for each single winding, and the related inverter. Also, the power flow only needs to go through 3 stages of power conversion (i.e. DC/AC, transformer, AC/DC) instead of 6 stages (i.e. DC/AC, transformer, AC/DC, DC/AC, transformer, AC/DC [16, 17]).

B. DC/AC segmented inverters for multiphase starter/generators

Historically, multiphase machines and drives became an attractive industrial solution in the last decades for the advantages that they can provide in terms of performance, fault tolerance and control for high power applications such as electric ship propulsion [18–22], wind farms [23], turbo compressors [24] and aircraft generating systems [25–27].

Nowadays, many efforts are being made to discover and fully exploit all the possibilities that this technology can provide.

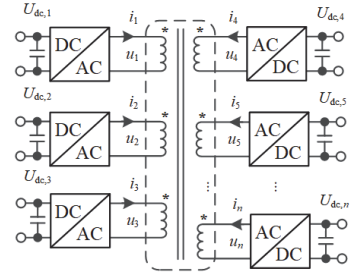


Fig. 3. Structure of MAB converters.

B. DC/AC segmented inverters for multiphase starter/generators

Historically, multiphase machines and drives became an attractive industrial solution in the last decades for the advantages that they can provide in terms of performance, fault tolerance and control for high power applications such as electric ship propulsion [18–22], wind farms [23], turbo compressors [24] and aircraft generating systems [25–27]. Nowadays, many efforts are being made to discover and fully exploit all the possibilities that this technology can provide.

From the basic principle, a multi-phase machine differs from a standard three-phase one for having a number of phases (m) higher than 3. This is possible and simple when the machine is fed by a power electronic converter with an arbitrary number of converter legs. Therefore, the number of machine phases results in a degree of freedom for the overall drive design.

The converter layout can be defined by choosing the number of independent sub-converters, how many phases are fed by each of them, and where the legs are connected to. An interesting solution for industrial applications is the one that exploits a set of three-phase converters to design the multiphase system, leading to the so called multi three-phase drive. This concept is well presented in Fig. 4, where the same machine is fed by a twelve-phase converter in Fig. 4(a) and a four three-phase one in Fig. 4(b). The neutral points are isolated, so that in the multi three-phase layout faults can be isolated. Also multi-leg layouts or multi H-bridges can be adopted. However, the clear advantage of a multi three-phase layout is that it allows the use of a well-known converter technology.

Not only the power electronics defines the capabilities of a multi-phase drive, but also the winding topology. Conventional three-phase windings are mainly categorized in: concentrated or distributed, full or short pitched, star or delta connected, single or double layer. However, a traditional three-phase machine always has three balanced phases (with same coil geometries) 120 electrical degrees shifted (symmetrical winding), with each phase mirrored under all the pole pairs (the related coils are then just series or parallel connected). These options are still available in a multiphase drive, but there are some new degrees of freedom. For example, an m -phase winding can still be based on equally distributed phases (shifted by $360/m$ electrical degrees) or can be distributed with a different angle (asymmetrical winding) [28, 29]. In particular,

considering a multi three-phase layout, if all the three-phase subsystems (balanced and symmetrical) are placed in the same electrical position it is said that the winding is without phase shift. Instead, if they are shifted by a certain angle the new winding is called phase-shifted [27]. Furthermore, the phases can be all identically placed under each machine stator pole pair or can be located in the same electrical positions but under different stator areas (sectors). This last category of multiphase windings is named as multi-sectored [30]. Finally, an interesting design of multiphase winding is the one based on a multi-winding layout. In this particular solution, more windings (generally two) are differently wound around the stator in order to control more harmonics of the air gap flux density. However, the advantages of this solution have been mainly exploited for not standard solutions such as bearing-less applications [31-33].

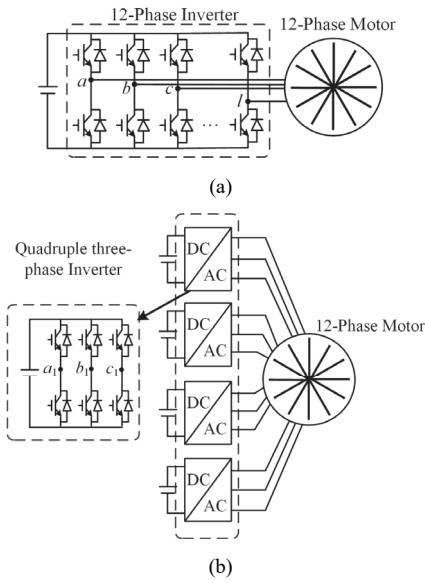


Fig. 4. Different configurations of multi-phase drives: (a) Conceptual scheme of a multiphase drive (twelve-phase), and (b) the respective multi three-phase layout (quadruple three-phase).

Considering the EPDS of Fig. 2, by replacing the main generators with segmented generators the total capacity, weight and volume of the generators, as well as the associated inverters, are not changed. In addition, performance, reliability and redundancy of the system are enhanced.

C. Fault tolerant strategies for the combined structure

A ring distribution of electric power is established by the combination of DC/DC MAB converters and DC/AC segmented inverters for starter/generators, where different power flow loops can be created to operate the system under different fault conditions. In particular, the main working operations of the system are summarized as follows:

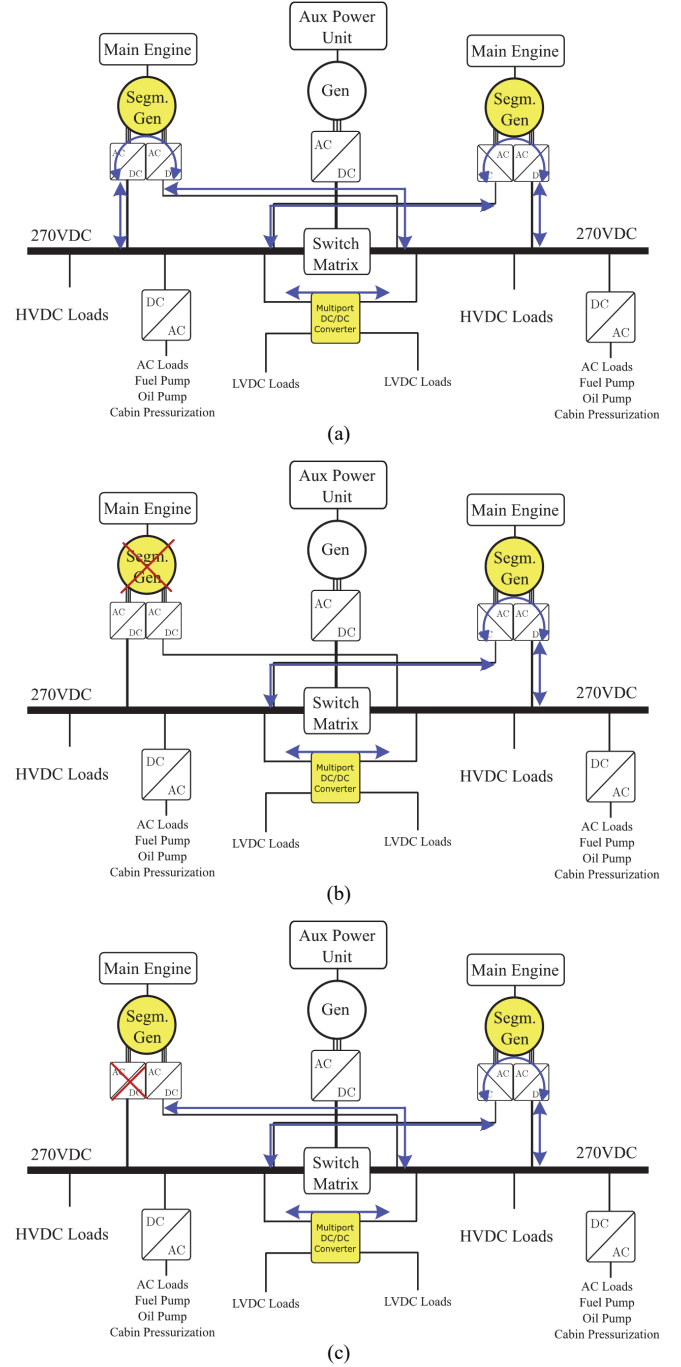
a) The segmented generator and inverters may provide full power to the DC bus in normal conditions, as shown in Fig. 5(a);

b) The configuration may provide 50% up to 100% of full power if any of the main engines is broken, as shown in Fig. 5(b);

c) The configuration may provide 75% up to 100% of full power if any of the segmented inverters is broken, as shown in Fig. 5(c);

d) The combination may provide 25% up to 50% of full power in condition of any main engine broken together with another segmented inverter broken, as shown in Fig. 5(d).

Consequently, in a similar way to MAB transformers, the use of multi three-phase segmented machine configurations not only provides enhanced performance and additional redundancy to the distribution system, but also ensures isolation between the 3-phase subsystems.



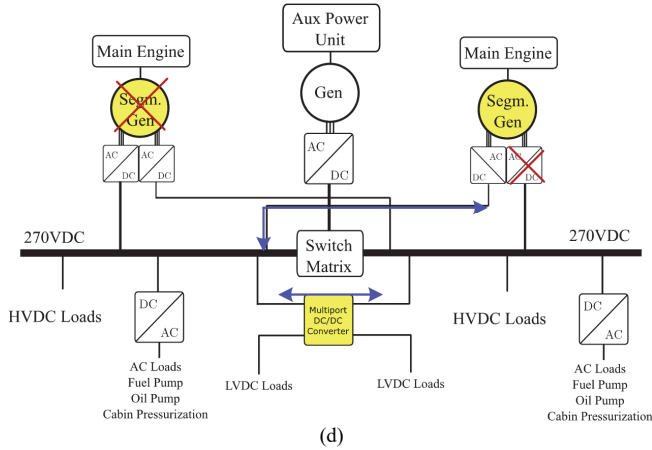


Fig. 5. Example of the proposed MPCS in different fault conditions: (a) no fault, (b) main engine or generator fault, (c) segmented inverter fault, (d) main engine or generator fault together with another segmented inverter fault.

D. Communication considerations of the units

For the MEA power distribution systems, optical fibers are used as information path. Optical fibers are point-to-point transmission media. Star-connected information network is one solution of communication and synchronization. The advantage of star-connected network is that the time delay of synchronization is very small, and the module redundancy is easily implemented by disabling the gate signal of the H-bridge and bypassing the target module.

Although the star-connected information network is well performed, the number of optical fibers is large and it is unfavourable for system modularity. A ring-connected information network is appropriate for the configuration shown in Fig. 2. The number of optical fibers is smaller than in star-connected networks, but the time delay of synchronization must be calculated during system operation. Module redundancy could be obtained by means of dual-ring-connected networks (both clockwise and anticlockwise).

III. AN EXAMPLE OF SEGMENTED MACHINE DESIGN FOR THE MPCS

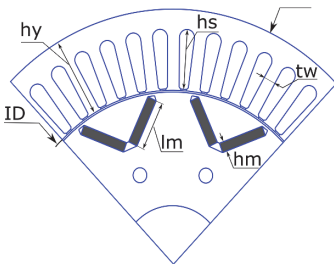


Fig. 6. Sketch of one pole pair of the IPM machine geometry.

This section presents a case study of machine analysis, aiming at highlighting the enhancement in the performance that can be reached transitioning from a single three-phase system to a multiple three-phase one. The electrical machine adopted in this system is an 8 poles interior permanent magnets (IPM)

machine with a V-Shape layout, as shown in Fig. 6. The main advantages of this machine are high torque and an extended power range capability over the base speed (namely flux weakening region). A summary of the machine parameters is given in Table I. The following analysis is mainly focused on the back electromotive force (EMF), torque and efficiency performance considering two different winding layouts: (a) A conventional 3-phase winding; (b) A double 3-phase winding (2×3 -phase).

TABLE I. MACHINE PARAMETERS.

Parameters	Values	Units
Number of poles	8	-
Number of slots	48	-
Number of conductors in the slot	8	-
Length steak (L_{stk})	110.0	mm
Outer stator diameter (D_{OUT})	203.0	mm
Inner stator diameter (D_{IN})	138.0	mm
Slot height (h_s)	25.07	mm
Back iron height (h_y)	33.1	mm
Tooth width (t_w)	5.2	mm
Airgap	0.7	mm
Magnet length (l_m)	20.0	mm
Magnet height (h_m)	4.0	mm
Cooling	natural convection	-
Magnets material	rare earth (NdFeB)	-

A. Torque analysis

Multi-phase design can give significant benefits in terms of ripple and average torque. Indeed, the control strategy of a multi-phase machine can be extended to the control of some high order space harmonics of the airgap magnetic field [34]. In addition, the winding factor is higher compared to a 3-phase winding [35], leading to a higher average torque. In this section, both torque and torque ripple have been carried out by means of finite element (FE) simulations, maintaining the same machines' overall volume and supply conditions.

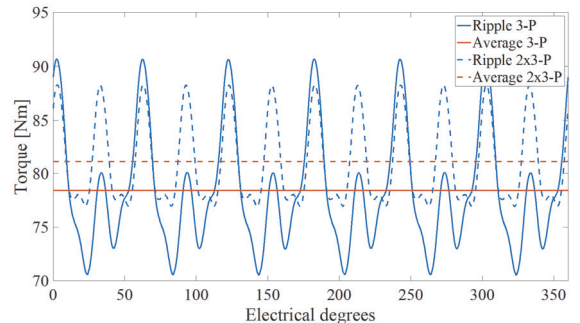


Fig. 7. Torque ripple comparison.

In Fig. 7 the torque ripple resulting from a different winding arrangement is shown: for 3-phase and 2×3 -phase distribution,

respectively. The results highlight that the 2×3-phase machine features an average torque of 81.1N·m with respect to the 78.4N·m in the 3-phase machine, with an overall increase of +3.40%. The multi three phase layout also helps in reducing the torque ripple. In the 3-phase case the peak to peak torque ripple is 25.58%, whereas it is 13.65% for the 2×3-phase motor, leading to an overall reduction of the oscillations by 11.93%, with respect to the single 3-phase winding machine.

B. Losses analysis

In literature, many researchers have been working on the estimation of the iron losses with analytical and FE models. In [36], an accurate prediction of iron losses for various frequencies and magnetic flux densities, considering the influence of higher order time harmonics and minor loops, is presented. In [37], an improved model of the iron losses for an induction machine based on a comparison of different equations has been developed. The influence of the pulse width modulation (PWM) generated by inverter on machine iron losses is also described in [38].

In this paper, in order to have a preliminary indication of the iron losses in the machine, the classical Steinmetz method is considered with the hypothesis of sinusoidal flux in the iron. This is used as a quantitative method for a comparative estimation of the iron losses expressed with the following equation:

$$P_{\text{iron}} = B_{\text{peak}}^2 (k_{\text{hy}} f + k_{\text{ed}} f^\alpha) \quad (1)$$

where B_{peak} is the maximum value of flux density in the iron, k_{hy} and k_{ed} are the hysteresis and eddy current coefficients, respectively, f is the frequency and α is the Steinmetz coefficient. However, considering a unique value of B_{peak} in the stator core does not permit to consider the asymmetrical flux density behavior. In fact, for a 3-phase machine presenting a number of slots/poles per phase $q > 1$ the flux density is not symmetrical due to high harmonic order fields generated by currents [39]. In this case, another advantage introduced by the 2×3-phase winding is that the number of slots/poles per phase is $q = 1$ so that the flux density results symmetrical in all stator core parts. The approach proposed takes into the account these asymmetries allowing for a better comparison between the two considered winding layouts.

The iron losses in the two consecutive teeth and on two consecutive yokes at the top of each area are calculated as follows:

$$\begin{cases} P_{\text{tooth1}} = k_t P_{\text{spec,iron}} B_{t1}^2 (k_{\text{hy}} f + k_{\text{ed}} f^\alpha) w_t \\ P_{\text{tooth2}} = k_t P_{\text{spec,iron}} B_{t2}^2 (k_{\text{hy}} f + k_{\text{ed}} f^\alpha) w_t \\ P_{\text{yoke1}} = k_y P_{\text{spec,iron}} B_{y1}^2 (k_{\text{hy}} f + k_{\text{ed}} f^\alpha) w_y \\ P_{\text{yoke2}} = k_y P_{\text{spec,iron}} B_{y2}^2 (k_{\text{hy}} f + k_{\text{ed}} f^\alpha) w_y \end{cases} \quad (2)$$

where $P_{\text{spec,iron}}$ takes into the account the specific iron losses in the core, while k_t , k_y , B_t , B_y , w_t and w_y are the correction coefficients, peak flux density values and weights related to the teeth and the volumes of back iron around the slots, respectively. Table II lists the parameters used for the FE

simulations.

TABLE II. SIMULATION PARAMETERS USED FOR IRON LOSS ANALYSIS.

Parameters	Value 3-phase
$P_{\text{spec,iron}}$ [W/kg]	2.30
k_{hy}	0.70
k_{ed}	0.30
f [Hz]	100
α	2
k_t	2
k_y	1.5
w_t	0.12
w_y	0.08

Finally, it is possible to obtain the total iron losses in the stator by applying the following equation (where Q_s is the total number of teeth of the machine):

$$P_{\text{iron,stator}} = \frac{Q_s}{2} (P_{\text{tooth1}} + P_{\text{tooth2}} + P_{\text{yoke1}} + P_{\text{yoke2}}) \quad (3)$$

TABLE III. COMPARISON RESULTS FOR IRON LOSSES.

Parameters	3-phase	2×3-phase
B_{t1} [T]	1.77	1.77
B_{t2} [T]	1.75	1.77
B_{y1} [T]	1.94	1.88
B_{y2} [T]	1.84	1.88
$P_{\text{iron,stator}}$ [W]	1.53	1.53

Table III summarizes the results obtained from the comparison of the two different winding arrangements. It is worth to highlight that, albeit the local saturation in the teeth of the 2×3-phase machine is more balanced, the overall stator iron losses are not significantly affected by the winding configuration.

C. Efficiency

The mechanical and rotor losses are neglected for simplicity in this qualitative evaluation exercise, as their contribution will only add an equal offset in the quantities of both analysed machines. The Joule losses have been calculated implementing the classical equation, function of the resistance R and phase current I_{rms} squared. In order to take into the account the additional losses such as eddy currents due to flux leakage in the machine housing and other parasitic losses, an additional loss, P_{add} , equivalent to 10% of the calculated Joule losses P_j is introduced. The efficiency is calculated as:

$$\eta = \frac{T_{\text{avg}} \Omega_b}{(T_{\text{avg}} \Omega_b) + P_{\text{iron,stator}} + P_j + P_{\text{add}}} \times 100\% \quad (4)$$

where T_{avg} is the average torque and Ω_b is the rotor mechanical pulsation corresponding to the machine base speed.

D. Results comparison

In this subsection a summary of the compared results between 3-phase and 2×3-phase systems is given, as reported in Table IV.

TABLE IV. COMPARATIVE ANALYSIS OF DIFFERENT WINDING CONFIGURATIONS.

Parameters	3-phase	2×3-phase	Units
Peak phase current I_{peak}	71.25	71.25	A
Joule losses P_j	39.10	39.10	W
Stator iron losses $P_{iron,sator}$	326	325	W
Additional Joule losses P_{add}	3.91	3.91	W
Total machine losses P_{tot}	369	368	W
Mechanical speed Ω_b	157.08	157.08	rad/s
Average torque T_{avg}	78.4	81.1	N·m
Machine output power P_{out}	12.32	12.74	kW
Machine efficiency η	97.10%	97.20%	-

It is worth to highlight that for the same current loading in the machine slots, the mechanical output power is higher with a multi-phase configuration (+3.4%), and consequently showing an improved torque capability. If the application is demanding a minimization of the volume, the machine can produce the same torque with the same current load and reduced volume. In fact, being the torque proportional to the stack length of the machine, the active stack length for the multi-phase machine can be reduced from $l_{3p} = 110.0$ mm (the active stack length of the 3-phase machine) to $l_{2\times 3p} = 106.3$ mm. This can lead to a weight reduction from 32.3 kg to 31.2 kg if a multi-phase winding is adopted. Therefore, for the same phase current and output torque, the multi-phase machine will result 1.10 kg lighter (about 3.4%). Furthermore, also the efficiency results to be slightly increased (about 0.10%) compared to the 3-phase solution.

IV. SIMULATIONS OF DIFFERENT FAULT SCENARIOS

The simulation model is developed based on Fig. 5 in Matlab/Simulink and PLECS Blockset with one segmented electrical machine and one quadruple active bridge (QAB) converter. The segmented machine is split into two 3-phase systems. Two of the DC ports of the QAB are connected to the segmented machine via two separate 3-phase half-bridge inverters, and the other two DC ports are connected to either DC loads or DC power sources. For the analysis, voltage V_{dc1} and V_{dc2} will be the Port 1 & Port 2 DC buses whereas V_{dc3} and V_{dc4} will represent the Port 3 & Port 4 DC buses of the QAB converter. Table V summarizes the main simulation parameters.

Considering that both the QAB and the segmented drives feature fully-bidirectional power electronics, connected to the same buses, different control strategies can be implemented. When multiple power converters have the capability of controlling the voltage, de-centralized control based on droop control has been widely adopted in the area of DC microgrid

and motor control [40]. This allows for the independent design of the control loops but may reduce the dynamic performance.

TABLE V. SIMULATION PARAMETERS.

Variables	Parameters and units
$V_{dc1}, V_{dc2}, V_{dc3}, V_{dc4}$	50V
L_1, L_2, L_3, L_4	30μH
C_1, C_2, C_3, C_4	1mF
f_{sw}	10kHz

A cascaded current and voltage control is therefore employed in the segmented drives as in a traditional rectifier control for machine. Each voltage control generates the current reference i_q^* for the respective part of the machine. Because there is more than one regulator that has the DC bus voltage V_{dc} as the control target, virtual resistors R_{v1} and R_{v2} are used for the grid stabilization, as shown in Fig. 8(a).

The QAB is controlled with a phase shift-control that has the LVDC voltage as the control target. Virtual resistor (R_{v1} and R_{v2}) control is used for the equalization of the power drawn from the HVDC buses, as shown in Fig. 8(b). A decoupling control as the one described in [12] can be implemented to reduce the influence of unbalanced power transfer among the ports on the dynamic performance. Having the balancing control also in the HV side of the QAB control allows for the voltage control of the HVDC bus even in the case of a double fault of the segments connected to the same bus. For the QAB parameters, the switching frequency is 10 kHz and the dc-link voltage is 50 V. As shown in Fig. 8(b), the parameters of the balancing controller are: $K_p = 0.005$, $K_i = 1$, whereas in the DC voltage controller they are: $K_p = 0.01$, $K_i = 1$, and the virtual resistance is set to 1 Ω. For the decoupling strategy, $d_{31} = \text{output of PI voltage controller1} + 0.5 d_{21}$; $d_{41} = \text{output of PI voltage controller2} + 0.5 d_{21}$.

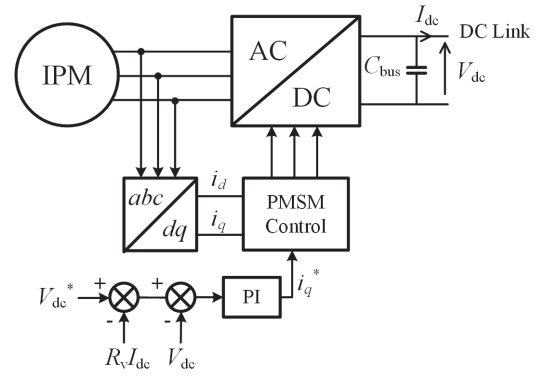
This control structure has the advantage that there is a complete redundancy in the control system in the case of a segmented machine failure. The independent voltage control allows for the automatic choice of the torque of each segment to balance the HVDC buses. In this way, the multi three-phase machine operates as a power router, exploiting the galvanic isolation of the windings to transfer power between the HVDC buses. The summary of operating conditions (generating or motoring) together with different fault conditions (IPM machine system cut off or QAB port cut off) are shown in Table VI.

For the generating mode, the double 3-phase IPM machine is connected to Port 1 and Port 2 of QAB through voltage source inverters. The speed of the simulated machine is constant (300 rpm). The Port 1 and Port 2 voltages are controlled by the machine controller via inverters separately. The machine segments are with double closed-loop control, for which the outer loop is with a reference of DC voltage, and inner loop with a reference of d-q current. The QAB is controlled following the diagram in Fig. 8(b), so that Port 1 and Port 2 power are balanced. Port 3 and Port 4 are connected to two resistive loads with resistance of 25 Ω and 25 Ω, respectively.

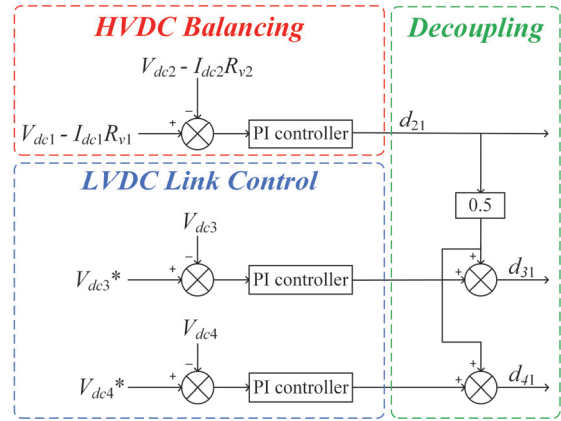
For the motoring mode, the double 3-phase IPM machine is connected to Port 3 and Port 4 of QAB through inverters. The Port 1 and Port 2 voltages are connected to the same DC voltage source, controlled at 50 V, by separated inverters. At the same time, the machine is torque controlled, by setting the d-q currents to $i_d = 0$ and $i_q = 3.3$ A, respectively. The QAB is controlled using the diagram in Fig. 8(b), so that Port 1 and Port 2 powers are kept balanced.

Fig. 9 illustrates the simulation results during normal operation. The two segmented inverters provide half of the load power each. Fig. 10 shows the simulation results of one segmented inverter open-circuit fault (at 0.4s) under motoring mode and generating mode, respectively. It is obvious that the DC voltage of the four port of the QAB is remaining the same (i.e. about 50V), while for motoring mode, one of the machine segment is cut off, and the power of another machine segment is doubled. Therefore, the DC supply power of Port 1 & 2 keep the same. The fault of one machine segment does not affect the power supply. For generating mode, one of the machine segment is cut off, and the power of another machine segment is doubled. Therefore, the DC supply powers of Port 1 and 2 are unchanged. The fault of one machine segment does not affect the DC loads.

Fig. 11 shows the simulation results for a disconnection of a QAB port (at 0.4s). It can be observed that the DC voltages of the four ports of the QAB remain the same (i.e. about 50V), whereas for motoring mode, one port of the QAB is disconnected, and the power of the other QAB port is doubled. Therefore, the power of the machine segments is kept constant. The fault of one QAB port does not affect the machine side. For generating mode, one of the QAB port is cut off, and the power of the other QAB port is doubled. Therefore, the power of the machine segments is not affected by the fault of one QAB port.



(a)



(b)

Fig. 8. Control of the multi-port distribution system: (a) the segmented machine with virtual resistor and (b) QAB with virtual resistor and voltage balancing.

TABLE VI. SUMMARY OF THE FAULT CONDITIONS FOR DIFFERENT OPERATING MODES.

	Motoring mode	Generating mode
Connections	Port 1 and Port 2 of QAB are connected to the same DC voltage source; Port 3 and Port 4 QAB are connected to two systems of a double 3-phase machine separately	Port 1 and Port 2 of QAB are connected to two systems of a double 3-phase machine separately; Port 3 and Port 4 QAB are connected to two resistive loads separately
Control strategies	QAB: as shown in the diagram Machine: d-q current control (single loop)	QAB: as shown in the diagram Machine: double closed-loop control of DC voltages and d-q currents
Normal operation (Normal)	0 to 0.8s: DC voltages, currents are balanced	0 to 0.8s: DC voltages, currents are balanced
One machine system cut off at 0.4s (Fault 1)	One machine system (a load) cut off (i.e. at Port 3 of the QAB) at 0.4s 0 to 0.4s: DC voltages, currents are balanced 0.4s to 0.8s: Port 1 & 2 voltages and currents are balanced; Port 3 power reduced to zero; Port 4 power doubled	One machine system (a source) cut off (i.e. at Port 1 of the QAB) at 0.4s 0 to 0.4s: DC voltages, currents are balanced 0.4s to 0.8s: Port 3 & 4 voltages and currents are balanced; Port 1 power reduced to zero; Port 2 power doubled
One QAB port cut off at 0.4s (Fault 2)	One QAB port (a source) cut off (i.e. at Port 2 of the QAB) at 0.4s 0 to 0.4s: DC voltages, currents are balanced 0.4s to 0.8s: Port 3 & 4 voltages and currents are balanced; Port 2 power reduced to zero; Port 1 power doubled	One QAB port (a load) cut off (i.e. at Port 4 of the QAB) at 0.4s 0 to 0.4s: DC voltages, currents are balanced 0.4s to 0.8s: Port 1 & 2 voltages and currents are balanced; Port 4 power reduced to zero; Port 3 power doubled

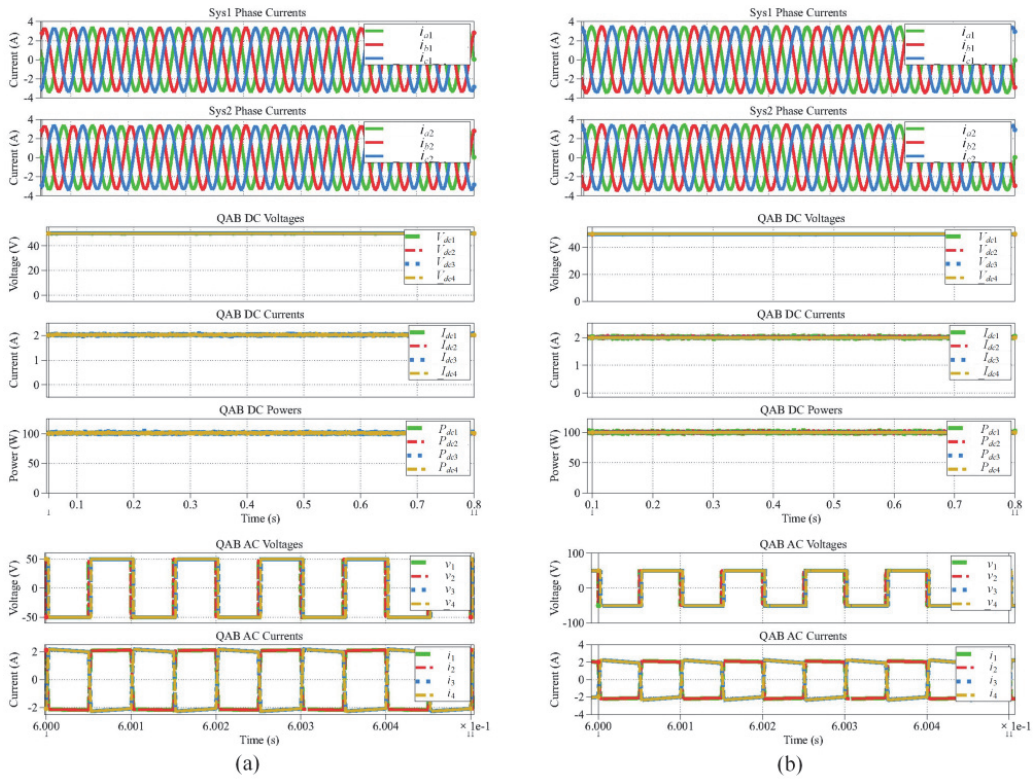


Fig. 9. Simulation results under normal operation. (a) Motoring mode. (b) Generating mode.

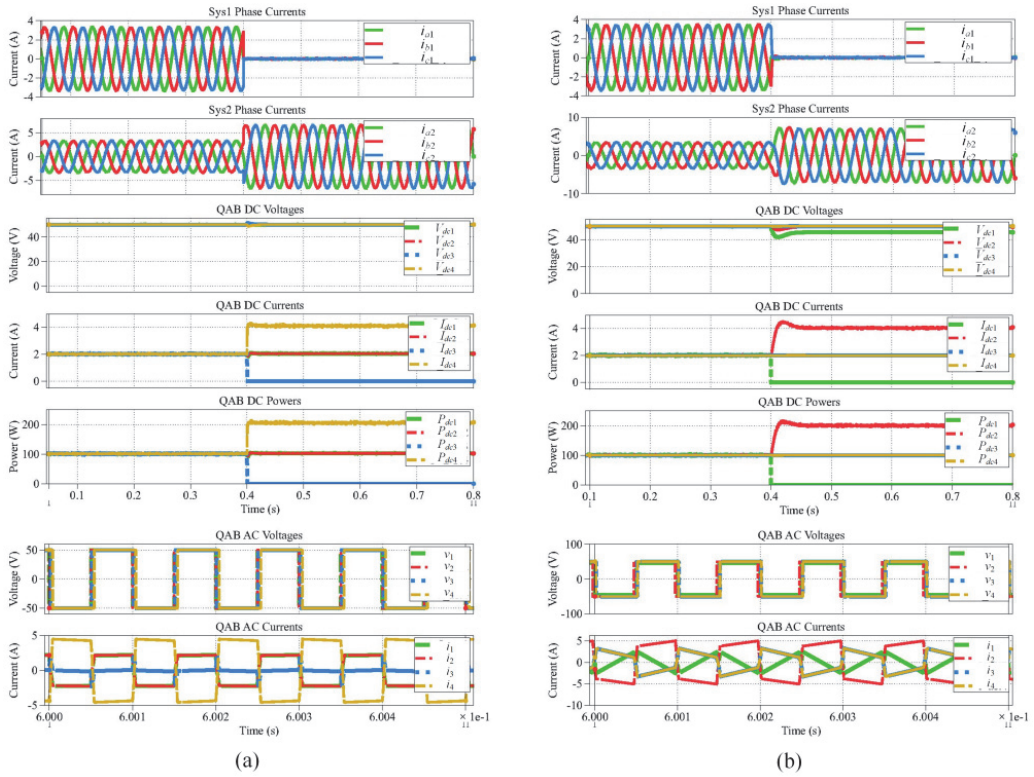


Fig. 10. Simulation results of one segmented machine system cut off at 0.4 s. (a) Motoring mode. (b) Generating mode.

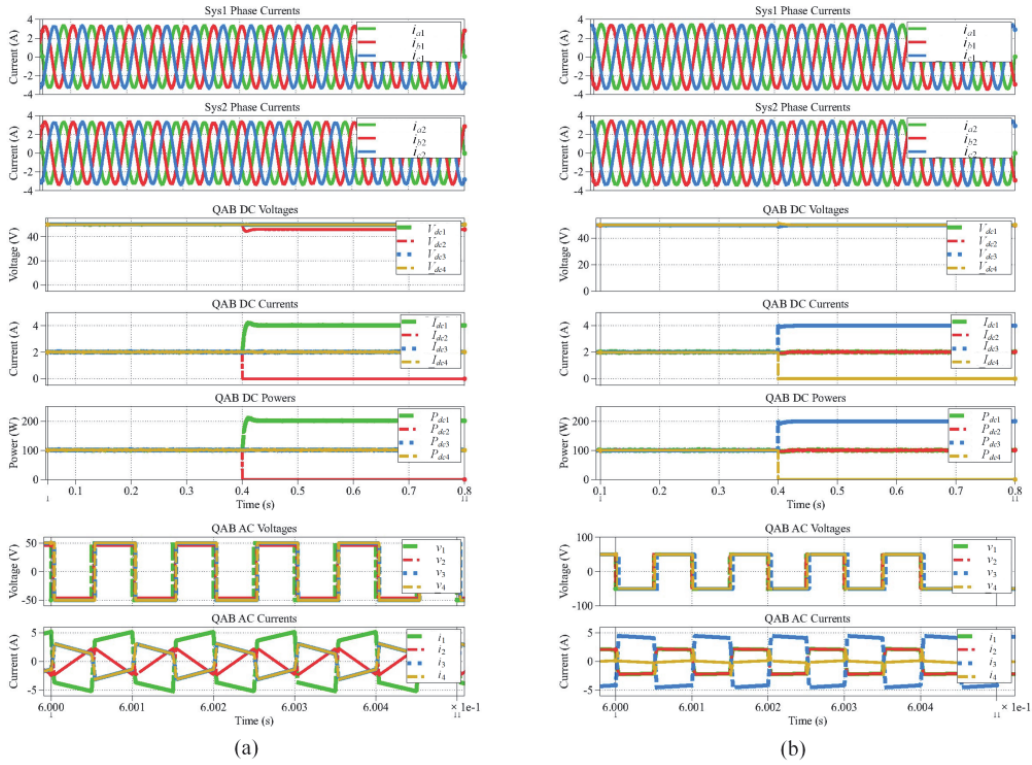
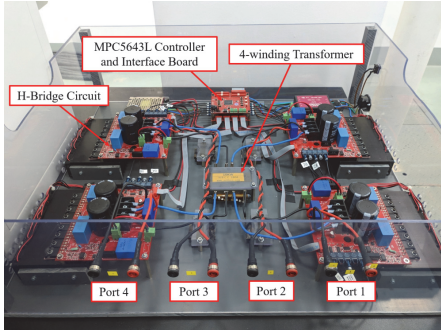
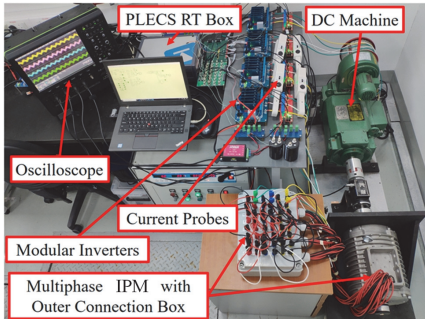


Fig. 11. Simulation results of a disconnection of a QAB port at 0.4 s. (a) Motoring mode. (b) Generating mode.

V. EXPERIMENTAL VERIFICATIONS



(a)



(b)

Fig. 12. Photos of the experimental prototype: (a) QAB converter, (b) segmented multiphase IPM machine and controllers.

The experimental verification of the proposed MPCs was implemented by connecting a QAB converter to the segmented multi-phase IPM machine, as illustrated in Fig. 2. The experimental platform is shown in Fig. 12, with the parameters in Table VII.

TABLE VII. EXPERIMENTAL PARAMETERS OF QAB.

Variables	Parameters and units
PWM frequency f_{sw}	10 kHz
DC voltage V_{dc1} , V_{dc2} , V_{dc3} , V_{dc4}	50 V
Communication speed	50 kB/s
K_p of balancing	0.005
K_i of balancing	1
K_p of voltage control	0.01
K_i of voltage control	1

The QAB is connected to the multi-phase IPM, where the 2×3 -phase machine and inverters work as DC loads with 2 isolated DC ports (i.e. exactly the same as the motoring mode of the simulation). The two ports of QAB on the secondary side (Port 3 & 4) are connected to the machine, and the other two ports (Port 1 & 2) of the QAB are connected to the DC power supply. The experimental results are aiming to demonstrate the power sharing capabilities offered by the multi-port converters. In fact, if the power electronics allows for unbalanced power processing, the scenarios presented in the simulation become possible. Table VIII shows the experimental parameters for the

test.

TABLE VIII. EXPERIMENTAL PARAMETERS OF MPCS.

Variables	Parameters and units
Speed	300 rpm
Pole pairs	4
DC voltages of QAB	50 V
Rated current of QAB	6.3 A
R_{v1} and R_{v2} for QAB control	1 Ω
Current reference	3.3 A
Inverter power switch	IKW75N60T
DC-link capacitor of Inverter	330 μ F

When it comes to the experimental configuration, as for the power supply side, two ports of the QAB converter are connected to two DC power supplies. As for the load side, other two ports are independently connected to two inverters to supply the dual three-phase machine. The control scheme of the experiment is the same as the one implemented in simulation for the motoring mode. The experiment can be divided into three parts: a) All ports of QAB converter are connected, the whole system is running with balance loads; b) A supply port of QAB converter is disconnected from DC power supply, the whole system is running with single DC source; c) A load port of QAB converter is disconnected from inverter, hence only one inverter is powered and the machine is running in single three-phase mode.

A. Experimental verification for balanced loads and power sources

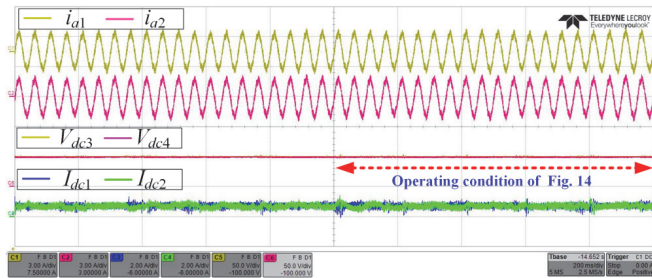


Fig. 13. Waveforms with all ports of QAB converter connected (normal condition).

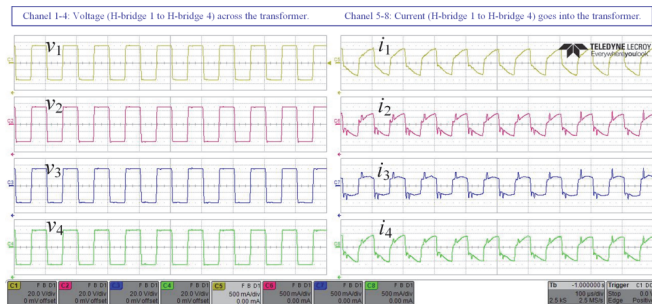


Fig. 14. Key waveforms of the QAB converter under normal condition.

To apply the decoupling control strategy in Fig. 8(b), the virtual resistance and the filter coefficients of the ADC into the DSP are changed. Fig. 13 shows the waveforms of the main quantities (currents and voltages) of the QAB converter under normal motoring operation of the electrical machine. Channel 1 and Channel 2 are the phase current of two segmented IPM machine systems, Channel 3 and Channel 4 are the currents of the two input ports from power supply, and Channel 5 and Channel 6 are the output voltage of QAB at the terminals of the two inverters. It can be seen that the currents of the two input ports are balanced.

Fig. 14 shows the QAB AC voltages and currents under normal condition. The phases of the square wave voltages are the same, therefore the AC currents of the 4 ports are similar, which also indicates the same power flow of the four ports.

B. Experimental verification for balanced loads but single power source

Fig. 15 shows the current and voltage waveforms when a source port of the QAB converter is disconnected and the power of the source at the other port is doubled. It can be observed that at the midpoint of timeline, the input current in Channel 3 goes up and the input current in Channel 4 falls down to make the input power constant. Meanwhile, the phase currents of the machine and the output DC voltage of the QAB converter do not change, indicating that the machine and the QAB are working well in the dual three-phase mode operation.

Fig. 16 shows the QAB AC voltages and currents under fault condition (one DC power source cut off). The phase of the square wave voltages are becoming different, therefore the AC currents of Port 1 is doubled, Port 2 is almost zero, and the current of Port 3 and 4 are not changed.

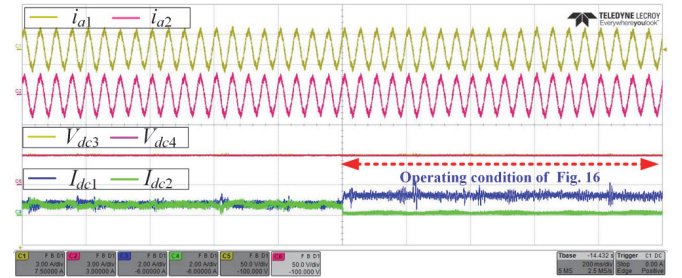


Fig. 15. The waveforms with one load port of QAB converter is disconnected (one load missing).

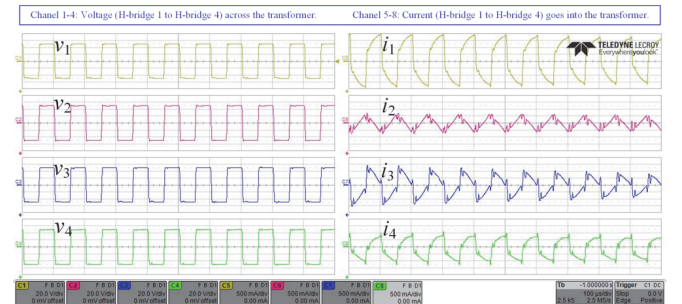


Fig. 16. Key waveforms of the QAB converter with one source port of QAB converter disconnected.

C. Experimental verification for balanced power sources but single load

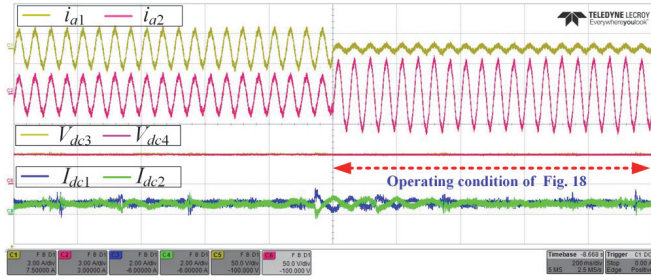


Fig. 17. The waveforms with one source port of QAB converter is disconnected (one sector of the machine is missing).

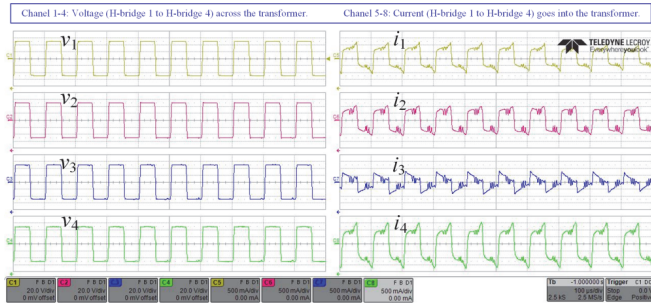


Fig. 18. Key waveforms of the QAB converter with one load port of QAB converter disconnected.

When a load port of QAB converter is disconnected from the inverter, the key waveforms are shown in Fig. 17. It can be observed that the phase currents of one inverter diminish while the phase currents of the other inverter increase, indicating that the operating mode of the machine is transferring from dual three-phase mode to single three-phase mode. The voltages of source ports of QAB converter keeps same. Furthermore, it can be seen from Channel 3 and Channel 4 that the input current of load ports has a drop at the midpoint of timeline and then increases to the new steady state, which can be attributed to the fact that the equilibrium point is changed between the two DC loads under the voltage droop control.

Fig. 18 shows the QAB AC voltages and currents under fault condition (one inverter load cut off). The phases of the square wave voltages are becoming different; therefore the AC current of Port 4 is doubled, at Port 3 is almost zero, and the currents of Port 1 and 2 do not change.

The results are showing the effectiveness of the proposed MPCS, which has been verified experimentally as shown in Fig 13 to 18. Fault tolerant operation is obtained as proposed in Fig. 5. With normal operating condition, the power of the two ports of the loads (inverters) are balanced, and the power of the two ports from the DC power sources are balanced, respectively. Thus, the power flow of each port is similar. With one source port of the QAB converter disconnected (as an emulation of the source fault), the power of the two systems of the segmented multi-phase machine are still balanced (no transient state of power control). With one load port of the QAB converter disconnected (as an emulation of the machine fault), the power of the two sources are always balanced. After a transient, the

healthy sector of the machine is carrying twice the power and the DC loads return to their normal operation. The time constant of the control is almost the same in simulations and experimental results, validating the control algorithm and the feasibility of the proposed system architecture.

VI. CONCLUSION

In this paper, the complete integration of multi-port converters for the electrical power distribution system of the MEA is carried out. This paper provides a novel concept to the EPDS on the MEA, integrating segmented machines and a multi-port MAB DC/DC converter for the bidirectional DC/AC conversion for starter/generators. The proposed MPCS for the MEA allows for the realization of a ring electrical power distribution, where the galvanic separation is guaranteed by the windings of the transformers in the MAB converters and the multi three-phase windings of the machines. This configuration shows its resiliency to faults in multiple scenarios and this is demonstrated by simulation results realized on a simplified grid. The experimental verification shows the evidence of the effectiveness of the MPCS. The results are focused on the unbalanced operation of a multi-three-phase machine and multiple active bridge converters, demonstrating how this technology can enable the flexible operation of the EPDS in the MEA.

REFERENCE

- [1] S. P. Engel, M. Stieneker, N. Soltau, S. Rabiee, H. Stagge and R. W. De Doncker, "Comparison of the Modular Multilevel DC Converter and the Dual-Active Bridge Converter for Power Conversion in HVDC and MVDC Grids," *IEEE Transactions on Power Electronics*, vol. 30, no. 1, pp. 124-137, Jan. 2015. doi: 10.1109/TPEL.2014.2310656.
- [2] G. Buticchi, L. Costa and M. Liserre, "Improving System Efficiency for the More Electric Aircraft: A Look at dc/dc Converters for the Avionic Onboard dc Microgrid," *IEEE Industrial Electronics Magazine*, vol. 11, no. 3, pp. 26-36, Sept. 2017. doi: 10.1109/MIE.2017.2723911.
- [3] T. Yang, S. Bozhko and G. Asher, "Functional Modeling of Symmetrical Multipulse Autotransformer Rectifier Units for Aerospace Applications," *IEEE Transactions on Power Electronics*, vol. 30, no. 9, pp. 4704-4713, Sept. 2015. doi: 10.1109/TPEL.2014.2364682.
- [4] S. Falcones, R. Ayyanar and X. Mao, "A DC-DC Multiport-Converter-Based Solid-State Transformer Integrating Distributed Generation and Storage," *IEEE Transactions on Power Electronics*, vol. 28, no. 5, pp. 2192-2203, May 2013. doi: 10.1109/TPEL.2012.2215965.
- [5] Z. Zheng, Z. Gao, C. Gu, L. Xu, K. Wang and Y. Li, "Stability and Voltage Balance Control of a Modular Converter With Multiwinding High-Frequency Transformer," *IEEE Transactions on Power Electronics*, vol. 29, no. 8, pp. 4183-4194, Aug. 2014. doi: 10.1109/TPEL.2013.2290019.
- [6] J. Yang, G. Buticchi, C. Gu, S. Günter, H. Zhang and P. Wheeler, "A Generalized Input Impedance Model of Multiple Active Bridge Converter," *IEEE Transactions on Transportation Electrification*. doi: 10.1109/TTE.2020.2986604.
- [7] C. Gu, et al., "Multi-Port Power Conversion Systems for the More Electric Aircraft," *IECON 2018 - 44th Annual Conference of the IEEE Industrial Electronics Society*, Washington, DC, 2018, pp. 5553-5558. doi: 10.1109/IECON.2018.8592915.
- [8] P. Wheeler and S. Bozhko, "The More Electric Aircraft: Technology and challenges," *IEEE Electrification Magazine*, vol. 2, no. 4, pp. 6-12, Dec. 2014. doi: 10.1109/MELE.2014.2360720.
- [9] J. Chen, C. Wang and J. Chen, "Investigation on the Selection of Electric Power System Architecture for Future More Electric Aircraft," *IEEE Transactions on Transportation Electrification*, vol. 4, no. 2, pp. 563-576, June 2018. doi: 10.1109/TTE.2018.2792332.

- [10] B. Karanayil, M. Ciobotaru and V. G. Agelidis, "Power Flow Management of Isolated Multiport Converter for More Electric Aircraft," *IEEE Transactions on Power Electronics*, vol. 32, no. 7, pp. 5850-5861, July 2017. doi: 10.1109/TPEL.2016.2614019.
- [11] C. Gu, Z. Zheng, L. Xu, K. Wang and Y. Li, "Modeling and Control of a Multiport Power Electronic Transformer (PET) for Electric Traction Applications," *IEEE Transactions on Power Electronics*, vol. 31, no. 2, pp. 915-927, Feb. 2016. doi: 10.1109/TPEL.2015.2416212.
- [12] G. Buticchi, L. F. Costa, D. Barater, M. Liserre and E. D. Amarillo, "A Quadruple Active Bridge Converter for the Storage Integration on the More Electric Aircraft," *IEEE Transactions on Power Electronics*, vol. 33, no. 9, pp. 8174-8186, Sept. 2018. doi: 10.1109/TPEL.2017.2781258.
- [13] L. F. Costa, G. Buticchi and M. Liserre, "Quad-Active-Bridge DC-DC Converter as Cross-Link for Medium-Voltage Modular Inverters," *IEEE Transactions on Industry Applications*, vol. 53, no. 2, pp. 1243-1253, March-April 2017. doi: 10.1109/TIA.2016.2633539.
- [14] J. L. F. Vieira, J. A. Oliver, P. Alou and J. A. Cobos, "Power converter topologies for a high performance transformer rectifier unit in aircraft applications," *2014 11th IEEE/IAS International Conference on Industry Applications*, Juiz de Fora, 2014, pp. 1-8. doi: 10.1109/INDUSCON.2014.7059403.
- [15] A. Rodríguez, A. Vázquez, D. G. Lamar, M. M. Hernando and J. Sebastián, "Different Purpose Design Strategies and Techniques to Improve the Performance of a Dual Active Bridge With Phase-Shift Control," *IEEE Transactions on Power Electronics*, vol. 30, no. 2, pp. 790-804, Feb. 2015. doi: 10.1109/TPEL.2014.2309853.
- [16] G. Buticchi, L. F. Costa, and M. Liserre, "Multi-port DC/DC converter for the electrical power distribution system of the more electric aircraft," *Mathematics and Computers in Simulation*, vol. 158, pp. 387-402, Apr. 2019. doi: 10.1016/j.matcom.2018.09.019.
- [17] G. Buticchi, L. Costa and M. Liserre, "DC/DC conversion solutions to enable smart-grid behavior in the aircraft electrical power distribution system," *IECON 2017 - 43rd Annual Conference of the IEEE Industrial Electronics Society*, Beijing, 2017, pp. 4369-4374. doi: 10.1109/IECON.2017.8216752.
- [18] J. Dai, S. W. Nam, M. Pande and G. Esmaceli, "Medium-Voltage Current-Source Converter Drives for Marine Propulsion System Using a Dual-Winding Synchronous Machine," *IEEE Transactions on Industry Applications*, vol. 50, no. 6, pp. 3971-3976, Nov.-Dec. 2014. doi: 10.1109/TIA.2014.2316361.
- [19] J. S. Thongam, M. Tarbouchi, A. F. Okou, D. Bouchard and R. Beguenane, "Trends in naval ship propulsion drive motor technology," *2013 IEEE Electrical Power & Energy Conference*, Halifax, NS, 2013, pp. 1-5. doi: 10.1109/EPEC.2013.6802942.
- [20] F. Scuiller, J. Charpentier and E. Semail, "Multi-star multi-phase winding for a high power naval propulsion machine with low ripple torques and high fault tolerant ability," *2010 IEEE Vehicle Power and Propulsion Conference*, Lille, 2010, pp. 1-5. doi: 10.1109/VPPC.2010.5729185.
- [21] C. Bassi, A. Tassarolo, R. Menis and G. Sulligoi, "Analysis of different system design solutions for a high-power ship propulsion synchronous motor drive with multiple PWM converters," *Electrical Systems for Aircraft, Railway and Ship Propulsion*, Bologna, 2010, pp. 1-6. doi: 10.1109/ESARS.2010.5665224.
- [22] L. Parsa and H. A. Toliyat, "Five-phase permanent magnet motor drives for ship propulsion applications," *IEEE Electric Ship Technologies Symposium, 2005.*, Philadelphia, PA, 2005, pp. 371-378. doi: 10.1109/ESTS.2005.1524702.
- [23] I. Zoric, M. Jones and E. Levi, "Arbitrary Power Sharing Among Three-Phase Winding Sets of Multiphase Machines," *IEEE Transactions on Industrial Electronics*, vol. 65, no. 2, pp. 1128-1139, Feb. 2018. doi: 10.1109/TIE.2017.2733468.
- [24] A. Tassarolo, G. Zocco and C. Tonello, "Design and Testing of a 45-MW 100-Hz Quadruple-Star Synchronous Motor for a Liquefied Natural Gas Turbo-Compressor Drive," *IEEE Transactions on Industry Applications*, vol. 47, no. 3, pp. 1210-1219, May-June 2011. doi: 10.1109/TIA.2011.2126036.
- [25] R. Bojoi, A. Cavagnino, A. Tenconi and S. Vaschetto, "Control of Shaft-Line-Embedded Multiphase Starter/Generator for Aero-Engine," *IEEE Transactions on Industrial Electronics*, vol. 63, no. 1, pp. 641-652, Jan. 2016. doi: 10.1109/TIE.2015.2472637.
- [26] A. Cavagnino, Z. Li, A. Tenconi and S. Vaschetto, "Integrated Generator for More Electric Engine: Design and Testing of a Scaled-Size Prototype," *IEEE Transactions on Industry Applications*, vol. 49, no. 5, pp. 2034-2043, Sept.-Oct. 2013. doi: 10.1109/TIA.2013.2259785.
- [27] G. Sala, P. Girardini, M. Mengoni, L. Zarri, A. Tani and G. Serra, "Comparison of fault tolerant control techniques for quadruple three-phase induction machines under open-circuit fault," *2017 IEEE 11th International Symposium on Diagnostics for Electrical Machines, Power Electronics and Drives (SDEMPED)*, Tinos, 2017, pp. 213-219. doi: 10.1109/DEMPED.2017.8062358.
- [28] A. Tassarolo, "Accurate Computation of Multiphase Synchronous Machine Inductances Based on Winding Function Theory," *IEEE Transactions on Energy Conversion*, vol. 27, no. 4, pp. 895-904, Dec. 2012. doi: 10.1109/TEC.2012.2219050.
- [29] A. Tani, M. Mengoni, L. Zarri, G. Serra and D. Casadei, "Control of Multiphase Induction Motors With an Odd Number of Phases Under Open-Circuit Phase Faults," *IEEE Transactions on Power Electronics*, vol. 27, no. 2, pp. 565-577, Feb. 2012. doi: 10.1109/TPEL.2011.2140334.
- [30] G. Sala, *et al.*, "Space Vectors and Pseudoinverse Matrix Methods for the Radial Force Control in Bearingless Multisector Permanent Magnet Machines," *IEEE Transactions on Industrial Electronics*, vol. 65, no. 9, pp. 6912-6922, Sept. 2018. doi: 10.1109/TIE.2018.2795590.
- [31] E. L. Severson, R. Nilssen, T. Undeland and N. Mohan, "Design of Dual Purpose No-Voltage Combined Windings for Bearingless Motors," *IEEE Transactions on Industry Applications*, vol. 53, no. 5, pp. 4368-4379, Sept.-Oct. 2017. doi: 10.1109/TIA.2017.2706653.
- [32] R. Oishi, S. Horima, H. Sugimoto and A. Chiba, "A Novel Parallel Motor Winding Structure for Bearingless Motors," *IEEE Transactions on Magnetics*, vol. 49, no. 5, pp. 2287-2290, May 2013. doi: 10.1109/TMAG.2013.2240279.
- [33] S. Serri, A. Tani and G. Serra, "Analytical model of radial forces considering mutual effects between torque and levitation current space vectors in 5-phase PM bearingless motors," *IECON 2013 - 39th Annual Conference of the IEEE Industrial Electronics Society*, Vienna, 2013, pp. 5142-5147. doi: 10.1109/IECON.2013.6699970.
- [34] L. Parsa, "On advantages of multi-phase machines," *31st Annual Conference of IEEE Industrial Electronics Society, 2005. IECON 2005.*, Raleigh, NC, 2005, pp. 1574-1579. doi: 10.1109/IECON.2005.1569139.
- [35] Y. Burkhardt, A. Spagnolo, P. Lucas, M. Zavesky and P. Brockerhoff, "Design and analysis of a highly integrated 9-phase drivetrain for EV applications," *2014 International Conference on Electrical Machines (ICEM)*, Berlin, 2014, pp. 450-456. doi: 10.1109/ICELMACH.2014.6960219.
- [36] S. Steentjes, G. von Pflingsten, M. Hombitzer and K. Hameyer, "Iron-Loss Model With Consideration of Minor Loops Applied to FE-Simulations of Electrical Machines," *IEEE Transactions on Magnetics*, vol. 49, no. 7, pp. 3945-3948, July 2013. doi: 10.1109/TMAG.2013.2244072.
- [37] G. Yang, Z. Cui and L. Song, "Analysis of iron losses in induction motor with an improved iron-loss model," *2014 IEEE Conference and Expo Transportation Electrification Asia-Pacific (ITEC Asia-Pacific)*, Beijing, 2014, pp. 1-4. doi: 10.1109/ITEC-AP.2014.6940945.
- [38] S. Xue, *et al.*, "Iron Loss Model for Electrical Machine Fed by Low Switching Frequency Inverter," *IEEE Transactions on Magnetics*, vol. 53, no. 11, pp. 1-4, Nov. 2017, Art no. 2801004. doi: 10.1109/TMAG.2017.2696360.
- [39] G. Sala, D. D. Gaetano, M. Degano and C. Gerada, "Asymmetrical Flux Density Distribution in Stator Teeth of Surface Permanent Magnet Machines," *2019 IEEE Workshop on Electrical Machines Design, Control and Diagnosis (WEMDCD)*, Athens, Greece, 2019, pp. 29-33. doi: 10.1109/WEMDCD.2019.8887831.
- [40] A. Galassini, A. Costabeber, M. Degano, C. Gerada, A. Tassarolo and R. Menis, "Enhanced Power Sharing Transient With Droop Controllers for Multithree-Phase Synchronous Electrical Machines," *IEEE Transactions on Industrial Electronics*, vol. 66, no. 7, pp. 5600-5610, July 2019. doi: 10.1109/TIE.2018.2868029.



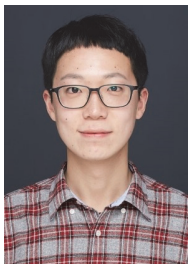
Chunyang Gu (M'15) was born in Heilongjiang, China, in 1988. She received BSc degree from Harbin Institute of Technology, Harbin, China, in 2010, and PhD degree from Tsinghua University, Beijing, China, in 2015, both in electrical engineering. In 2015, she went to the University of Nottingham, UK, where she was a postdoc research fellow in Power Electronics, Machines and Control (PEMC) Research Group. Since 2017, she has been an Assistant Professor in Department of Electrical and Electronic Engineering and PEMC Research Group, University of Nottingham Ningbo China. Her research interests include power electronics for transportation electrification, renewable energy and grid applications, e.g. solid-state transformer, solid-state circuit breaker, multi-level converter topologies and control, application of wide-band-gap semiconductor devices, power electronics in EV, railway, marine and MEA.



Hao Yan (M'18) received the B.S., M.S. and Ph.D. degrees in electrical engineering from the Harbin Institute of Technology, Harbin, China, in 2011, 2013 and 2018, respectively.

He subsequently joined the Power Electronics, Machines and Control Group, University of Nottingham, Ningbo, China, and worked on power electronics for electrical drives for two years. He is currently a Research Fellow with the Rolls-Royce @ NTU Corporate Lab, Nanyang Technological University, Singapore 639798. His current research

interests include permanent-magnet machine drives and power converters in More Electric Aircraft.



Jiajun Yang (S'18) received the B.Eng. degree (Hons.) in electrical and electronic engineering in 2017, from the University of Nottingham Ningbo China, Ningbo, China, where he is currently working toward the Ph.D. degree with the Key Laboratory of More Electric Aircraft Technology of Zhejiang Province.

From 2017 to 2018, he was a hardware engineer with the Nottingham Electrification Centre. His current research interests include high power density dc-dc converters and stability analysis of dc microgrids for the more electric aircraft.



Giacomo Sala received the B. Sc. in Power Engineering in 2012 the M. Sc. degree with honors in Electrical Engineering in 2014 and the Ph. D. in Electrical Machines and Drives in 2018 from the University of Bologna, Italy. He worked as a researcher until 2019 in the Power Electronics, Machines and Control Group, Department of Electrical and Electronic Engineering, The University of Nottingham.

He is currently a researcher in the Department of Electrical, Electronic, and Information Engineering "Guglielmo Marconi" - DEI, University of Bologna, Italy. His research interests include design, modelling and control of multiphase electrical machines, fault tolerant controls and fault diagnosis of electric drives.



Daniele De Gaetano received the Laurea degree in Electrical Engineering from the University of Napoli "Federico II", Napoli, Italy, in 2016 and the Laurea Magistrale degree in Electrical Energy Engineering from the University of Padova, Padova, Italy, in 2018. Currently, he is a PhD Student at University of Nottingham in the Power Electronics, Machines and Control (PEMC) Group.

His main research interests include design, modelling and analyses of multi-phase machines for high torque

capability applications.



Xuchen Wang (S'19) was born in Taizhou, China, in 1993. She received her B.Eng. (Hons.) degree in electrical and electronic engineering from the University of Nottingham Ningbo China in 2015. In 2019, she obtained the Ph.D. degree from the University of Nottingham in Electrical Engineering. She is currently a researcher with the department of electrical and electronic engineering (PEMC group), at the University of Nottingham. Her research interests include design, modelling and control of multiphase drives.



Alessandro Galassini (M'17) received the master's degree in mechatronic engineering from the University of Modena and Reggio Emilia, Reggio Emilia, Italy, in 2012, and the Ph.D. degree in power sharing for multi three phase electrical machines from the University of Nottingham, Nottingham, U.K., in 2017.

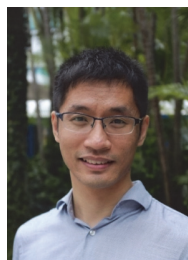
He is currently a Researcher with the Power Electronics, Machines and Control Group, University of Nottingham. His research area is focused on control

of electrical drives for future transportation systems.



Michele Degano (M'15) received his Master's degree in Electrical Engineering from the University of Trieste, Italy, in 2011, and his Ph.D. degree in Industrial Engineering from the University of Padova, Italy, in 2015. Between 2014 and 2016, he was a post-doctoral researcher at The University of Nottingham, UK, where he joined the Power Electronics, Machines and Control (PEMC) Research Group.

In 2016 he was appointed Assistant Professor in Advanced Electrical Machines, at The University of Nottingham, UK. He was promoted Associate Professor in 2020. His main research focuses on electrical machines and drives for industrial, automotive, railway and aerospace applications, ranging from small to large power. He is currently the PEMC Director of Industrial Liaison leading research projects for the development of future hybrid electric aerospace platforms and electric transports.



Xin Zhang (SM'20) received the Ph.D. degree in Automatic Control and Systems Engineering from the University of Sheffield, U.K., in 2016 and the Ph.D. degree in Electronic and Electrical Engineering from Nanjing University of Aeronautics & Astronautics, China, in 2014.

From February 2014 to December 2016, he was a Research Associate with The University of Sheffield. From January 2017 to September 2017, he was a Post-Doctoral Research Fellow with the City University of Hong Kong, Hong Kong. He is currently an Assistant

Professor of power engineering with the School of Electrical and Electronic Engineering, Nanyang Technological University, Singapore. He is generally interested in power electronics, power systems, and advanced control theory, together with their applications in various sectors.

Dr. Zhang has received the Highly Prestigious Chinese National Award for Outstanding Students Abroad in 2016.

He is the Associated Editor of IEEE TIE/JESTPE/OJPE/Access and IET Power Electronics.



Giampaolo Buticchi (SM'17) received the Master degree in Electronic Engineering in 2009 and the Ph.D degree in Information Technologies in 2013 from the University of Parma, Italy. In 2012 he was visiting researcher at The University of Nottingham, UK. Between 2014 and 2017, he was a post-doctoral researcher, and Guest Professor at the University of Kiel, Germany. During his stay in Germany, he was awarded with the Von Humboldt Post-doctoral Fellowship to carry out research related to fault tolerant topologies of smart transformers.

In 2017 he was appointed as Associate Professor in Electrical Engineering at The University of Nottingham Ningbo China and as Head of Power Electronics of the Nottingham Electrification Center. He was promoted to Professor in 2020. His research focuses on power electronics for renewable energy systems, smart transformer fed micro-grids and dc grids for the More Electric Aircraft. Dr. Buticchi is one of the advocates for DC distribution systems and multi-port power electronics onboard the future aircraft.

He is author/co-author of more than 210 scientific papers, an Associate Editor of the IEEE Transactions on Industrial Electronics, the IEEE Transactions on Transportation Electrification and the IEEE Open Journal of the Industrial Electronics Society. He is currently the Chair of the IEEE Industrial Electronics Society Technical Committee on Renewable Energy Systems.